PAPER

PHYSICAL ANTHROPOLOGY

Pierre Guyomarc'h,[1,2] *Ph.D.; Bruno Dutailly,*[1] *M.Sc.; Jérôme Charton,*[3] *M.Sc.; Frédéric Santos,*[1] *M.Sc.;*
Pascal Desbarats,[3] *Ph.D.; and Hélène Coqueugniot,*[1,4] *Ph.D.*

Anthropological Facial Approximation in Three Dimensions (AFA3D): Computer-Assisted Estimation of the Facial Morphology Using Geometric Morphometrics*

ABSTRACT: This study presents Anthropological Facial Approximation in Three Dimensions (AFA3D), a new computerized method for estimating face shape based on computed tomography (CT) scans of 500 French individuals. Facial soft tissue depths are estimated based on age, sex, corpulence, and craniometrics, and projected using reference planes to obtain the global facial appearance. Position and shape of the eyes, nose, mouth, and ears are inferred from cranial landmarks through geometric morphometrics. The 100 estimated cutaneous landmarks are then used to warp a generic face to the target facial approximation. A validation by re-sampling on a subsample demonstrated an average accuracy of *c.* 4 mm for the overall face. The resulting approximation is an objective probable facial shape, but is also synthetic (i.e., without texture), and therefore needs to be enhanced artistically prior to its use in forensic cases. AFA3D, integrated in the TIVMI software, is available freely for further testing.

KEYWORDS: forensic science, facial reconstruction, facial reproduction, soft tissue depth, TIVMI, computed tomography

Following the recommendations of the Scientific Working Group for Forensic Anthropology (SWGANTH), the aim of facial approximation is to (i) estimate antemortem facial appearance, (ii) suggest identity, and (iii) capture public attention. Current methods of facial approximation, however, rarely meet all three of these objectives, all of which are integral to the overarching goal of identification. The main critiques of current facial approximation techniques include: the inherent subjectivity in manual methods, lack of standardization, and poor correlations between facial bony structures and facial soft features, which limit the accuracy of the estimation (1–4). Although facial soft tissue depth (FSTD) studies, and more systematic evaluations of guidelines for reconstructing facial organs (i.e., eyes, nose, mouth, and ears), have been increasing during the last decade, the development of holistic approaches in computerized facial approximation is only in its beginning stages (5). Tradi-

tionally, FSTD is the main data explored in facial approximation, even if it only allows for an estimation of the general facial appearance of a subject based upon the skull. Using group-specific datasets, where choice relies on biological factors (e.g., age, sex, population, corpulence), has nevertheless been discussed in terms of statistical pertinence and visual impact (6). The facial organs are of utmost importance in the facial recognition process, (7) and recent research underlined the lack of reliability in the actual guidelines for the estimation of the shape, size, and position of such features (8–11). This aspect of facial approximation needs thorough investigation to assess correlations between soft tissues and craniofacial architecture.

Compared with manual methods, automation of facial approximation offers increased objectivity and the possibility of standardization. Despite significant evolutions during the last 15 years (12–15), there is still no computer-assisted tool to aid facial approximation that is globally accepted by the forensic community. A recent review of computerized craniofacial reconstruction methods by Claes et al. (16) offers an interpretation and classification of the methodology available and in development. Following their typology (see Table 1 in [16]), we propose a new holistic method, using a single generic face, based on craniofacial information from both the skull and the face extracted from computed tomography (CT) scans of 500 French individuals. The warping of the model is face-specific, using landmarks as boundaries around facial organs, completed by FSTD application between these features. This method is implemented via the computer program Anthropological Facial Approximation in 3D (AFA3D) which is part of the Treatment

[1]Université Bordeaux 1, UMR 5199 PACEA, CNRS, MCC, Anthropologie des Populations Passées et Présentes, F-33615 Pessac, France.
[2]Joint POW/MIA Accounting Command, Central Identification Laboratory, 310 Worchester Ave, Bldg 45, USA-96853, Joint Base Pearl Harbor-Hickam HI.
[3]Laboratoire Bordelais de Recherche en Informatique, Université Bordeaux 1, UMR 5800 LaBRI, 351 cours de la Libération, F-33405 Talence, France.
[4]Department of Human Evolution, Max Planck Institute for Evolutionary Anthropology, Deutscher Platz 6, D-04103 Leipzig, Germany.

TABLE 1—*Definition of the landmarks and dispersion intra- and interobserver (in mm).*

Landmark			Nature	Definition	Intra	Inter
Bone	Glabella*	g	Median	Most anterior midline point on the frontal bone	1.2	1.6
	Nasion*	n	Median	Midline point on the nasofrontal suture	0.6	0.6
	Mid-nasal*	mn	Median	Midline point on the internasal suture midway between nasion and rhinion	0.8	1
	Rhinion*	rhi	Median	Midline point at the inferior free end ot the internasal suture	0.4	0.7
	Nasospinale superior	nss	Median	Midline point on the inferior border of the piriform aperture at the intermaxillary suture	1	1.2
	Subspinale	ss	Median	Inferior midline point at the maximum of curvature of the nasal spine	1.2	3
	Akanthion	ak	Median	Most anterior midline point of the nasal spine	0.3	1
	Mid-philtrum*	mp	Median	Midline point midway between the base of the nasal spine and the prosthion	0.9	1.3
	Prosthion	pr	Median	Midline point at the most anterior edge of the superior alveolar ridge of the maxillae	0.8	1
	Incisor superior	is	Median	Midline point on the tangent of the inferior borders of the central superior incisors	1.2	1.6
	Infradentale	id	Median	Midline point at the most anterior edge on the inferior alveolar ridge ot the mandible	0.6	1
	Labiomentale*	labm	Median	Deepest midline point in the groove superior to the mental eminence	0.8	1.2
	Pogonion*	pg	Median	Most anterior midline point on the mental eminence of the mandible	1	1.1
	Supragnathion*	sgn	Median	Most antero-inferior midline point of the mental eminence between the pogonion and gnathion	1.1	1.5
	Gnathion*	gn	Median	Most inferior midline point at the mental symphysis of the mandible	0.9	0.9
	Frontotemporale*	ft	Bilateral	Most antero-medial point of the linea temporalis superior	1.3	1.8
	Zygion*	zy	Bilateral	Most lateral extent of the lateral surface of the zygomatic arch	1.8	2.5
	Porion	po	Bilateral	Central point on the upper margin of the external auditory meatus	1.2	1.9
	Mastoidale	ms	Bilateral	Most inferior point of the mastoid process	1	1.1
	Zygotemporale superior	zts	Bilateral	Most superior point of the zygomatico-temporal suture	0.6	1
	Zygotemporale inferior	zti	Bilateral	Most inferior point of the zygomatico-temporal suture	0.7	1.8
	Jugale*	ju	Bilateral	Most antero-inferior point on the posterior border of the zygomatic bone	0.8	1.4
	Frontomalare temporale*	fmt	Bilateral	Most posterior point of the zygofrontal suture	1	1.3
	Frontomalare orbitale	fmo	Bilateral	Most anterior point of the zygofrontal suture on the orbital rim	1.1	1.2
	Superciliare*	sci	Bilateral	Most anterior point of the supraciliary arch in the axe of the center of the orbit	1.3	2
	Maxillofrontale	mf	Bilateral	Point at the intersection of the fronto-maxillary suture and the anterior lacrimal crest	1.6	1.9
	Supraconchion*	sk	Bilateral	Most superior point of the orbital rim	1.4	2.9
	Ectoconchion*	ec	Bilateral	Lateral point of the orbital rim, opposed to the maxillofrontale	2.1	3.2
	Orbitale*	or	Bilateral	Most inferior point of the orbital margin	1.1	2
	Zygoorbitale*	zo	Bilateral	Point of the zygomaxillary suture on the orbital rim	0.9	1.8
	Nasomaxillofrontale	nmf	Bilateral	Point at the intersection of the frontal, maxillary, and nasal bones	1.1	1.3
	Mid-nasomaxillaire*	mnm	Bilateral	Point of the nasomaxillary suture between the nasomaxillare and the nasomaxillofrontale	1.5	1.8
	Nasomaxillare*	nm	Bilateral	Most inferior point of the nasomaxillary suture on the nasal aperture	1.3	1.7
	Apertion	ap	Bilateral	Most lateral point of the piriform aperture	2.1	3.2
	Piriform curvature	cp	Bilateral	Most infero-lateral point of the piriform aperture	0.9	1.3
	Nariale	na	Bilateral	Most inferior point of the piriform aperture	0.7	1.1
	Zygomatic*	za	Bilateral	Most salient point of the zygomatic on the zygomatic major muscle insertion	2.1	5.2
	Zygomaxillare*	zm	Bilateral	Most inferior point on the zygo-maxillary suture	1.5	1.9
	Canine Fossa*	cf	Bilateral	Most postero-medial (deepest) point of the maxilla in the supra canine fossa	2.7	6.1
	Submaxillar curvature*	csm	Bilateral	Most supero-medial point on the maxillary inflexion between the zygomaxillare and the ectomolare	1.6	3.7
	Condylion*	co	Bilateral	Most lateral point of the glenoid process of the mandible	1.4	1.9
	Koronion	kr	Bilateral	Most superior point on the coronoid process of the mandibular ramus	1	1.1
	Gonion*	go	Bilateral	Most postero-inferior point of the lateral border of the mandiblule	1.7	2
	Mid-ramus*	mr	Bilateral	Point at the center of the mandibular ramus	2.7	3.5
	Ectomolare*	ecm	Bilateral	Point on the superior alveolar ridge superior to the crown of the maxillary second molar	0.9	1.1
	Supra canine*	sc	Bilateral	Point on the superior alveolar ridge superior to the crown of the maxillary canine	1.1	1.5
	Inframolare*	im	Bilateral	Point on the inferior alveolar ridge inferior to the crown of the mandibular second molar	1.2	1.4
	Infra canine*	ic	Bilateral	Point on the inferior alveolar ridge inferior to the crown of the mandibular canine	1.2	1.5
	Mental foramen*	fm	Bilateral	Most anterior point of the border of the mental foramen	0.6	0.8
	Mid-mandibular border*	mmb	Bilateral	Point on the inferior border of the corpus of the mandible midway between gonion and pogonion	2.1	3.9
	Mid-mandibular body*	mmc	Bilateral	Point on the center of the corpus of the mandible located on the oblique line	3.2	5
Skin	Pronasale	prn	Median	Most anterior midline point of the nose	0.5	0.6
	Inferonasale	in	Median	Most antero-inferior midline point of the nose	0.6	0.7
	Midseption	msep	Median	Midline point of the columella between the two nostrils	0.5	1.4
	Subnasale	sbn	Median	Most postero-supérior midline point of the nasal septum (maximum of curvature)	1.4	1.8
	Labrale superior	ls	Median	Midline point on the vermillion border of the superior lip	1.3	1.4
	Stomion	sto	Median	Midline point between the lips (only when the mouth is closed)	0.6	0.9
	Labrale inferior	li	Median	Midline point on the vermillion border of the inferior lip	1.1	1.2
	Exocanthion	ex	Bilateral	Lateral point of the outer corner of the eye fissure	1.2	3.1
	Endocanthion	en	Bilateral	Medial point of the inner corner of the eye fissure	0.7	2.9
	Palpebrale inferior	pi	Bilateral	Central point of the anterior border of the inferior eyelid	0.9	1.6
	Oculus anterior	oa	Bilateral	Most anterior point of the eyeball (taken on a transverse DICOM slice)	1	1.8
	External alar curvature	eac	Bilateral	Most anterior point of the nasal wing at the maximum of curvature	1.8	2.6
	Superior alar curvature	sac	Bilateral	Most superior point of the nasal wing	1.6	2.3
	Alagenion	ag	Bilateral	Most posterior point of the nasal wing	1.5	1.5

TABLE 1—Continued.

Landmark		Nature	Definition	Dispersion	
				Intra	Inter
Alare	al	Bilateral	Most lateral point of the nasal wing	1.9	2.9
Alacrepidon	ac	Bilateral	Most inferior point of the nasal wing in anterior view	1	1.3
Section	sep	Bilateral	Medial point of the nostril, at the smallest width of the nasal septum	0.4	1.4
Philtrum colonna	pc	Bilateral	Point of the vermillion border of the superior lip, at the basis of the philtrum column	0.9	1.2
Cheilion	ch	Bilateral	Most lateral point of the mouth fissure, where both lips meet	0.8	2.1
Otobasion superior	obs	Bilateral	Point of attachment of the helix in the temporal region	1.2	2.3
Superaurale	sa	Bilateral	Most superior point on the free margin of the auricle	1.5	1.7
Postaurale	pa	Bilateral	Most posterior point on the free margin of the auricle	2.5	2.6
Subaurale	sba	Bilateral	Most inferior point on the free margin of the auricle	1.3	2.4
Otobasion inferior	obi	Bilateral	Point of attachment of the ear lobe to the cheek	0.9	1.4
Protragion	prt	Bilateral	Most posterior point of the tragus	0.8	0.9

*Indicates the bony landmarks that were used to produce FSTD landmarks by automatic projection on soft tissues.

and Increased Vision for Medical Imaging (TIVMI) software. AFA3D requires the user to position 78 three-dimensional (3D) landmarks to independently estimate the FSTD and the shape of the facial organs through geometric morphometrics. This study presents the methods that led to the development of AFA3D and the accuracy of the produced approximations (for further details, see [17], primary manuscript in French available at http://www.theses.fr/2011BOR14354).

Material and Methods

Computed Tomography (CT) Scans

With the help of radiologists, numerous craniofacial CT scans (c. 1000), of individuals of know age and sex, were collected in 2008 and 2009 directly from French hospitals and medical center archives. Ethical approval for the collection was obtained from the French *Comité de protection des personnes (Sud-Ouest et Outre Mer III)*. From the collected scans, only adult (>18 years) patients free of facial trauma and pathology were retained for analysis. The resulting sample of 500 individuals homogeneously covered all sexes (265 males, 235 females) and age groups (age range: 18–96 years, mean = 52 years, SD = 20; with approximately the same number of males and females in each decennial age group: 18–29, 30–39, 40–49, 50–59, 60–69, 70–79, 80 and older). Figure 1 presents the sample size and geographical repartition.

All patients were scanned in the supine position, but facial patterns varied (e.g., eyes/mouth closed or opened). Because complete craniofacial CT scans (from the chin to the vertex) are not systematically required (i.e., the facial region scanned usually depends on the clinical problem), half of the 500 individuals showed a relatively complete scan (from the chin to the glabella), while the other half displayed only partial scans (c. 2/3 of the superior face and 1/3 of the inferior face). Integration of the partial scans allowed for a larger sample size, permitting facial features/FSTD to be studied independently on different subsamples. For the above-mentioned reasons, and because of the variable facial patterns exhibited by the patients, landmark data were recorded only on the available "neutral region" of the face (i.e., areas without facial expression or pressure due to medical equipment). The CT scan files were collected in anonymous Digital Imaging and Communications in Medicine (DICOM) format, which includes the spatial and density information for each slice, the restricted patient data (age and sex), and the settings used for the exam. The CT scans were selected to ensure that the space
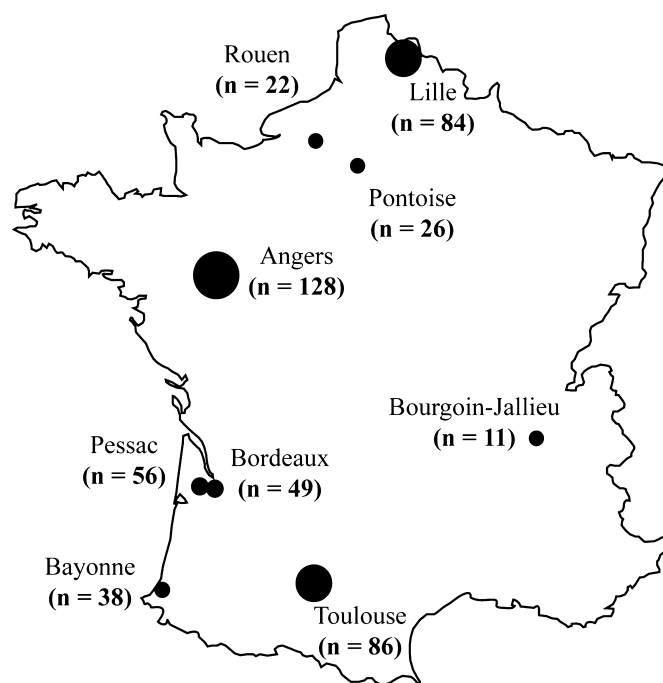

FIG. 1—*Localization of the nine French medical centers who provided the study's material and sample size.*

between slices was less than the slice thickness (insuring visualization of all anatomical structures). Settings depended on the scanner and the acquisition parameters of the sample, but all CT scans had an average slice thickness of <1 mm (ranging from 0.6 to 1.5 mm) and a between-slice space of <0.7 mm (ranging from 0.3 to 1 mm).

Treatment and Increased Vision for Medical Imaging (TIVMI)

Digital Imaging and Communications in Medicine files were processed by TIVMI, free software available online for educational and research purposes (http://projets.pacea.u-bordeaux.fr/TIVMI/), and developed by one of the authors (BD). TIVMI was designed to evolve through a system of plug-ins, adapting to the needs of anthropological research using medical imaging, 3D visualization, and measurements. In addition to classic geometric operations (e.g., landmark positioning, plane, line, segment construction, etc.), TIVMI allows for the reconstruction of 3D surfaces from DICOM files, applying the half-maximum

height algorithm (HMH, see [18]) in three dimensions (19). Each facial surface (soft and hard tissues) was reconstructed with this protocol, ensuring an accurate detection of the interface between different tissues and creating a reproducible rendering of the patient's anatomy (Fig. 2). The reliability of the surface reconstruction process used in this study has been previously assessed (see [20]), minimizing the uncertainty of measurement at the source of AFA3D methodology.

Landmarks

Landmark (type I, II, and III [21]) data were chosen for the AFA3D method because of its ease of use and practicability in interpretation. Classic cranial and facial landmarks were selected to cover the different surfaces of the skull and face as much as possible. The selection followed the facial approximation literature to preserve homology and comparability between studies. A total of 189 landmarks (described in Table 1, illustrated in Fig. 3) were used, including 87 bony landmarks and 102 soft tissue landmarks that consisted of both sensory landmarks (i.e., positioned on the facial organs) and FSTD landmarks (i.e., projected on the skin from the corresponding bony landmark). As the geometrically defined landmarks (i.e., type II and III) may be difficult to position directly on the 3D surfaces with accuracy, reference planes were constructed to guide the process. To ensure a correct orientation of the planes, the original definition of the Frankfurt Horizontal was used. Using both porions and both orbitales, four planes were created using the different combinations of three landmarks and an average of those four planes defines a strictly horizontal plane or mean horizontal (MH) plane. A mean coronal (MC) plane was constructed by averaging two planes orthogonally to MH and passing by the porions and the orbitales, respectively. Finally, the mean sagittal (MS) plane was built orthogonally to MH and MC, passing through nasion (Fig. 4). In TIVMI, planes can be visualized and shifted to extremities (e.g., MC is shifted up to the most anterior part of the frontal bone, the glabella landmark is then position at the intersection of this region and the MS). Reference planes were used to position most of the type II and III landmarks, notably enhancing their repeatability and reproducibility.

The uncertainty of measurement was assessed for intra- and interobserver positioning by calculating the dispersion (average distance between the mean position of a landmark and the repeated measurements) for each landmark. Five sets of landmarks were taken five times by one observer with a week interval between each set, and 20 sets of landmarks were taken by two observers. Results are presented in the Table 1. Special care must be taken when positioning the landmarks with a high interobserver error when using AFA3D (hence definitions, with screenshots, are provided within the user manual). The analysis and consequent method described in this study may nevertheless be subject to intra-observer position variation. Landmarks showing significant intra-observer variation were mainly used for the FSTD data, and their use was limited in the geometric morphometrics analyses.

Facial Soft Tissue Depths (FSTD)

The approximation of the global facial appearance is obtained by the application of FSTD. Even if the use of a single pooled dataset is valid (6), the method chosen for AFA3D is to apply individual-specific thicknesses. For a complete description of the methodology for FSTD, see (22) (raw data available at www.craniofacialidentification.com). Corpulence is the main influence on facial soft tissues and bears more weight in this regard than age, sex, or population. As the body mass index (BMI) was unknown for the sample, normal *versus* overweight BMI categories have been estimated using principal component analyses (PCA) on FSTD of the cheek region. This allowed for the classification of the 500 individuals into one of the two categories, and the consequent distribution within age and sex was found to be consistent with demographic data of the modern French population (23). Regression equations were constructed with age, sex, corpulence, and craniometrics as independent variables to estimate the most probable FSTD at 37 landmarks for the target individual (22). As biological factors are used as dichotomous variables (e.g., female = 0; male = 1), it was not necessary to select a category if the factor was indeterminate (e.g., the value of 0.5 was used in the regressions if the sex was unknown). Craniometric variables were extracted automatically after the positioning of bony landmarks by the user and applied (along with the biological factors specified) to the equations integrated in AFA3D. As the FSTD were measured perpendicularly to the reference planes, the soft tissue landmarks were projected following the reference plane at the calculated length of the FSTD. This first operation produced 59 FSTD landmarks that define the most probable general facial size and shape of the target individual.

Facial Organs Estimation

Geometric morphometrics (GMM) are a set of statistical tools used for the analysis of form, defined by size and shape, through different methods, including landmark data processed by Procrustes superimposition (24–27). GMM was used in this study to assess the correlations between sets of bone landmarks and sets of sensory landmarks (i.e., positioned on eyes, nose, mouth, and ears). All analyses were performed using version 1.02 m of MorphoJ software (28). The evaluation of covariation in facial elements was performed with Two Blocks Partial Least Squares (PLS) analyses, after the division of the craniofacial architecture in different matrices. Subdivision of the regions was essential for the following: (i) including partial CT scans in the sample, (ii)
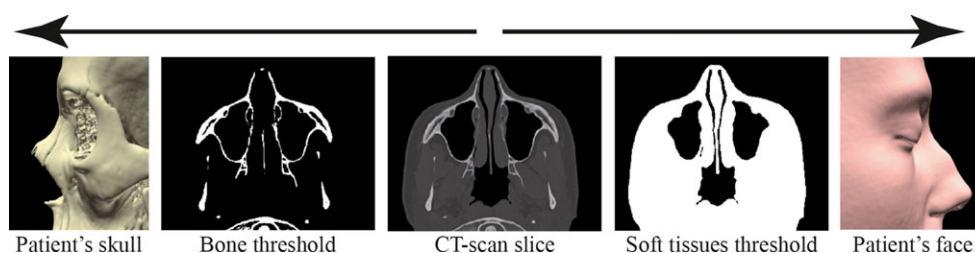

FIG. 2—*Extraction of three-dimensional surfaces from CT scans using the HMH 3D algorithm (19) in TIVMI.*
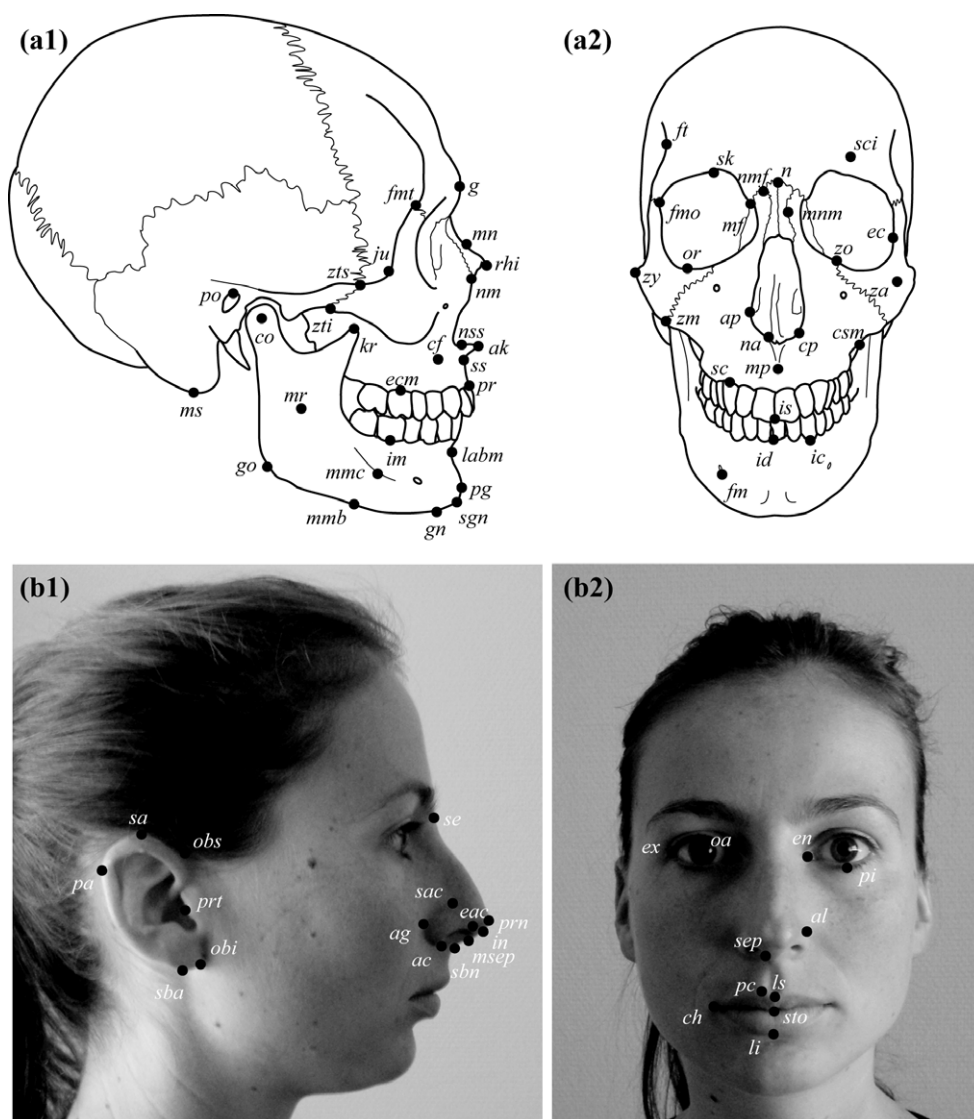
FIG. 3—*Bony landmarks in lateral (a1) and anterior (a2) views; cutaneous sensory landmarks in lateral (b1) and anterior (b2) views. See Table 1 for abbreviation and definition.*

keeping the number of variables low enough relatively to the sample size to obtain solid results/interpretations, and (iii) having a more precise understanding of the shape variability within a specific anatomical region. The functional matrices (following the hypothesis formulated by Moss and Young [29]) are displayed in the Fig. 5. Both sides of the symmetrical matrices (right and left) were tested independently. PLS explains the amount of covariance between two sets of landmarks and provides an RV coefficient, analogous to the coefficient of determination (30–33). Functioning similarly to PCA, PLS provided a visualization of the related variations between the two blocks after decomposition of the main shape components in different axes. Each cutaneous matrix was compared with each bony matrix to find the best correlation. The covariations concerned homogeneous position changes of the landmarks, which could be identified by vectors of translation; the length of those vectors thus revealed the most correlated landmarks. A specific bony estimation matrix was finally built upon the most correlated landmarks for each cutaneous matrix, optimizing the correlation between the two sets. The four new matrices then served as the basis for the estimation of the shape of the facial organs.

The influences of sex, age, and size (allometry) on the shape components for each of the four pairs of correlated matrices were evaluated with discriminant function analyses (DFA) and multivariate regressions. Understanding and quantifying the impact of such factors will eventually help to improve the estimation model. Asymmetry was also explored by applying the analyses independently on the symmetric and asymmetric parts of the configurations, to determine if each side should be analyzed separately or not.

Principal component analyses were used to simplify the data and create independent principal component (PC) scores that quantify the different shapes studied. After a partial Procrustes Superimposition (objects are translated and rotated, but not scaled), each matrix was subjected to PCA, and PC scores accounting for 95% of the shape variations were stored. The bony PC scores and the factors of sex, age, and centroid size were used to build a model estimating the PC scores of the cutaneous matrix (through multivariate regression). Each obtained score was multiplied by the specific coefficient of the corresponding PCA and added to the x, y, and z coordinates of the consensus shape. This operation resulted in the most proba-
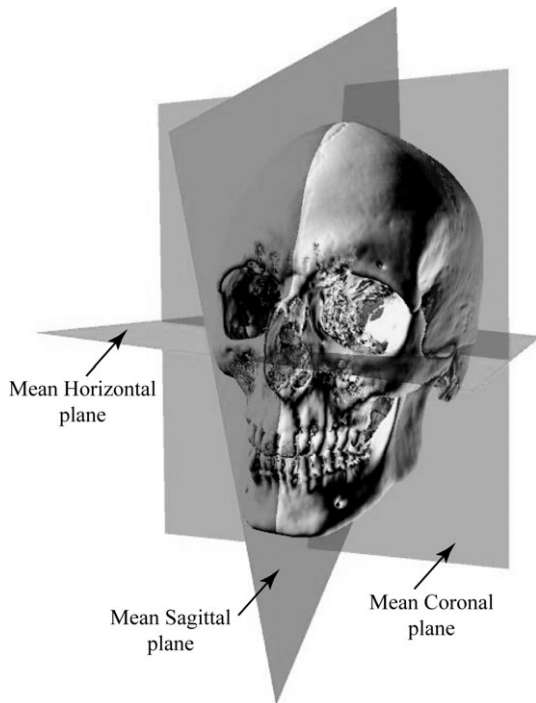
FIG. 4—*Reference planes built from the Frankfurt Horizontal.*

ble 3D coordinates of each sensory landmark of the target face, based on the sample of 500 French individuals. The calculation was independently processed for the eyes, nose, mouth, and ears.

Results

Exploratory Form Analyses

Table 2 summarizes the exploratory PLS results found for each comparison. The pattern of correlation followed an anatomical logic, the optical matrix correlated with the mid-superior face, the buccal matrix with the mid-inferior face, and the auditory matrix with the lateral parts of the skull. The respiratory matrix showed significant correlations with most of the matrices. The longest vectors of bony landmarks in the correlated matrices (those that display the highest amount of correlation with the cutaneous landmarks) were used to create the optimal estimation matrices (Figs 6–9). The landmarks that presented redundant correlations were extracted to keep the matrices with less variables and better estimation potential (only one of the analyses is graphically presented for each matrix, all figures and detailed results can be viewed in [17]).

The PLS results for the estimation matrices (Table 3) indicated that the correlations obtained are high for the nose region, moderate for the mouth and ears, and relatively low in the region of the eyes. It was noted that with a high sample size ($n > 100$), the RV coefficient attained a maximum correlation at *c.* 0.3, meaning that RV = 0.25 indicated a high correlation between the matrices. An example of correlation for the two-first PLS axes is depicted in Fig. 6. Homogeneous shape variations correlated between bony and cutaneous landmark configurations were extracted and classified in main axes. The first two to four PLS axes generally account for the main variations. The first PLS axis for the nose region illustrated that a thinner soft nose

is linked with a narrow face and nasal aperture, and an anterior projection of the tip/base of the soft nose is linked with anterior projection of the nasal bones and nasal spine. The second PLS axis accounted for 15% of the covariation and indicated other shape changes complementary to the first PLS, explaining further individualization of the soft nose shape.

Sexual dimorphism was significant (according to DFA) for all bony and cutaneous matrices, except for the facial inferior bony matrix (Table 3). Figure 7 shows the average differences between males and females in the auditory and facial lateral matrices. The angle formed by the two mandibular branches was more obtuse in females, and the axis porion-coronion was more horizontal than in males. A similar change of angle is detected on the external ears, which also tended to be wider in females. As sex has a significant influence on craniofacial shape, integrating it into the estimation is necessary for improvement of the model. The nasal and eye regions also presented similar sexually dimorphic patterns in bone and cutaneous landmarks groups.

The influence of age was also significant (according to DFA between individuals of <40 years and individuals of more than 40 years) for all matrices, except the facial superior bony matrix (Table 3). Figure 8 displays the shape changes related to age in the facial inferior and buccal matrices. Lips tended to get thinner with age, which can be related in part to loss of teeth and alveolar receding. Even if significant, age changes are relatively subtle for the three other facial regions. Nevertheless, if known, age can explain some shape changes and contribute to the shape individualization of the target face, particularly on the mouth.

The influence of size on shape, or allometry (tested by multivariate regression), was another factor positively significant on all matrices, except on the facial inferior matrix (Table 3). Size explained up to 9% (for the auditory matrix) of shape difference throughout the sample. Figure 9 displays allometrical variations in the facial superior and optical matrices. If the superior part of the skull was larger than the average, the glabella region was more anteriorly projected, and the eyes slightly wider, with more projected inferior eyelid (when the centroid size was significant). Size is a factor automatically collected on the bony matrices after Procrustes superimposition, so it can be easily used to improve the estimation model. In some instances, size was redundant with sexual dimorphism. As males tend to be larger than females, the shape sexual dimorphism quantified in geometric morphometrics includes static allometric sexual dimorphism (34). Nevertheless, the pattern was different for the mouth region, which justifies the use of centroid size as an estimator of its cutaneous shape.

Results provided significant findings for both symmetric and asymmetric parts in the sex, age, and allometry correlation analyses (results not presented here, available in [17]). Including both right and left parts in the estimation matrices of the eyes and the ears allowed for the accounting of the laterality-specific shape variations.

AFA3D

Implementation—As the CT scan material used to create the facial approximation method was processed in TIVMI, it appeared convenient to add it as a free module in the same software. The user needs to enter the 3D coordinates of the 78 bony landmarks (nine original landmarks were excluded after analyses due to redundancy in the estimation process) into AFA3D. Landmarks can be entered directly in the module after reconstruction of the target skull from a CT scan or as an importation of a 3D laser
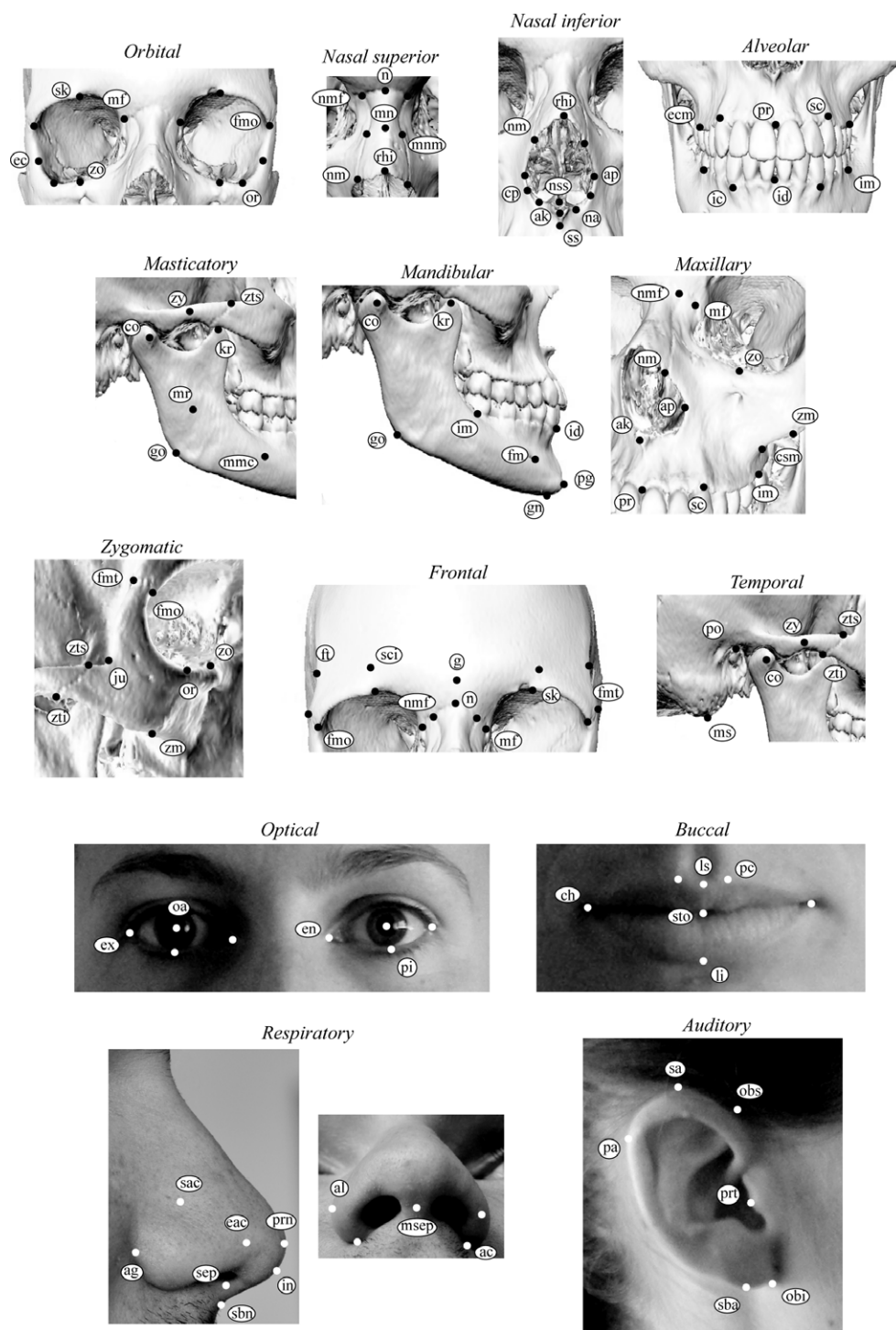
FIG. 5—*The ten osseous and four cutaneous matrices tested in the study for covariation. See Table 1 for abbreviation and definition.*

scanned surface. The raw coordinates may also be imported from a file after collection using another device (e.g., digitizer). The advantage of using TIVMI for landmark recording is the availability of the reference planes to ensure a more accurate positioning of the type II and III landmarks. A manual is provided on the TIVMI website to help the practitioner to correctly position the landmarks (http://projets.pacea.u-bordeaux.fr/TIVMI/index.php?page=a-fa3d). The mandible must be articulated with the cranium, in normal occlusion, and the missing data have to be estimated prior to the use of AFA3D. If the biological factors are known,

sex (male or female), age (below or over 40 years), and corpulence (normal or overweight) can be specified. Using only two categories for age is statistically adequate for the FSTD estimation and is more realistic regarding the age ranges that result from forensic anthropology age estimation methods. Those three factors can be left as "unknown" to produce average results.

As estimation of the skin landmarks was automatic, the FSTD was first calculated with the multivariate regression equations (22), and the corresponding FSTD landmarks were projected on the skull. The results of the FSTD estimation gave a mean stan-

TABLE 2—*Significant correlation between bony and cutaneous matrices tested by Two Blocks Partial Least Square Analyses (+: significant at p < 0.05).*

MATRIX	Optical	Respiratory	Buccal	Auditory
Orbital	+	+	−	+
Nasal superior	−	+	+	−
Nasal inferior	+	+	−	−
Alveolar	−	+	+	−
Masticatory	−	−	+	+
Mandibular	−	+	+	+
Maxillary	−	+	+	−
Zygomatic	+	+	+	−
Frontal	+	+	−	−
Temporal	−	+	+	+

dard error of the estimate (SEE) of 2.2 mm, with a maximum at gonion (4.9 mm) and a minimum at rhinion (0.9 mm). The SEE was systematically lower than the standard deviation of the mean for each FSTD, indicating that the use of regression equations resulted in more accurate estimations. (for results, see [22]). The sensory landmarks estimation was then independently performed in R (35) and processed by a portable version of R linked with TIVMI. The bony landmarks of the target skull were divided into the four estimation matrices and incorporated into the reference sample before performing PCA. The PC scores for the target skull were then extracted and entered into the model for estimation of the cutaneous PC scores, which were eventually converted into the approximated 3D landmark coordinates. The partial Procrustes superimpositions are aligned on the landmark
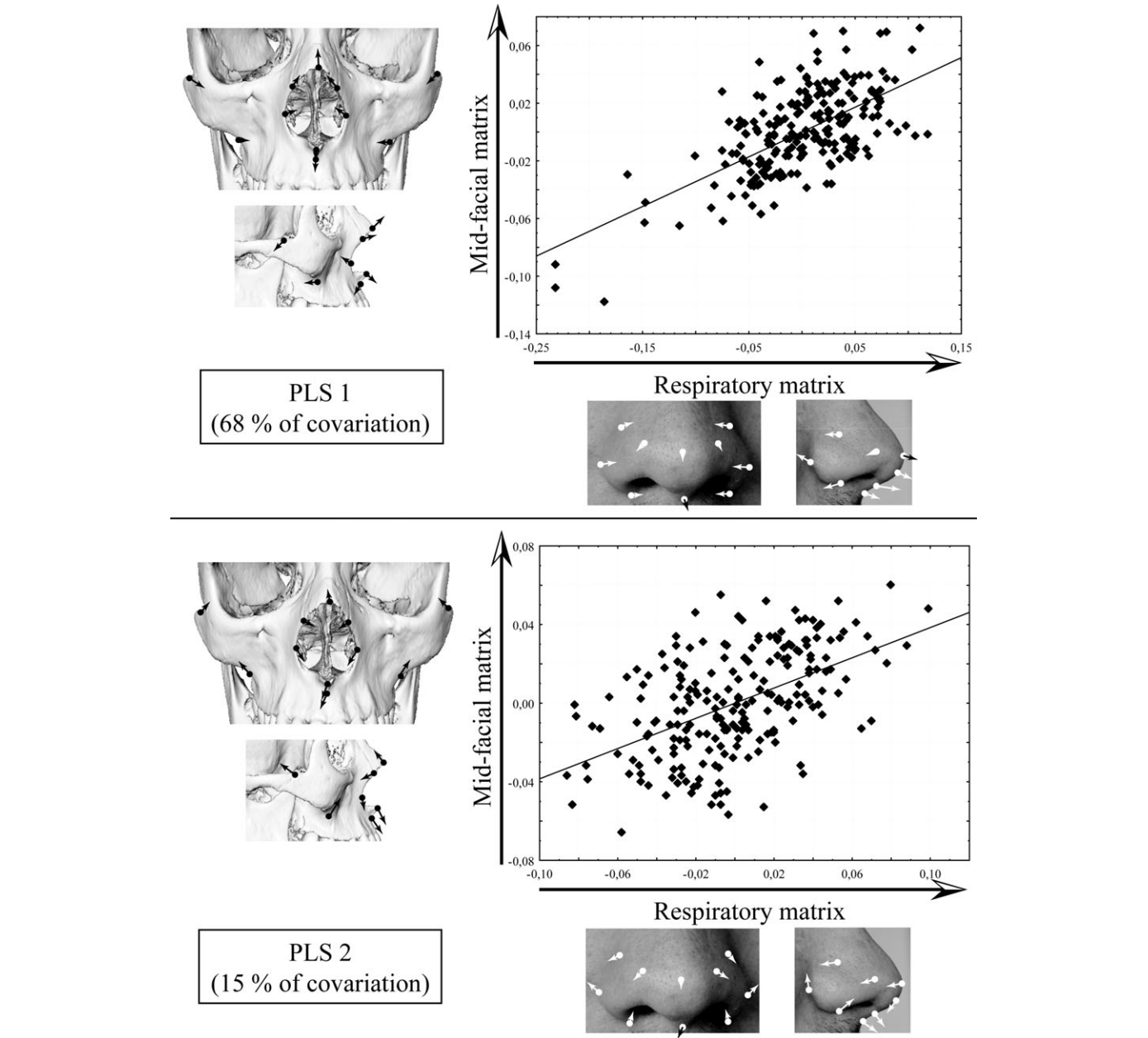

FIG. 6—*Covariation of the nasal region tested by Two Blocks Partial Square Analysis (PLS). The mid-facial matrix scores are correlated with the respiratory matrix scores, respectively, representing shape variations on the skull and the soft tissues.*
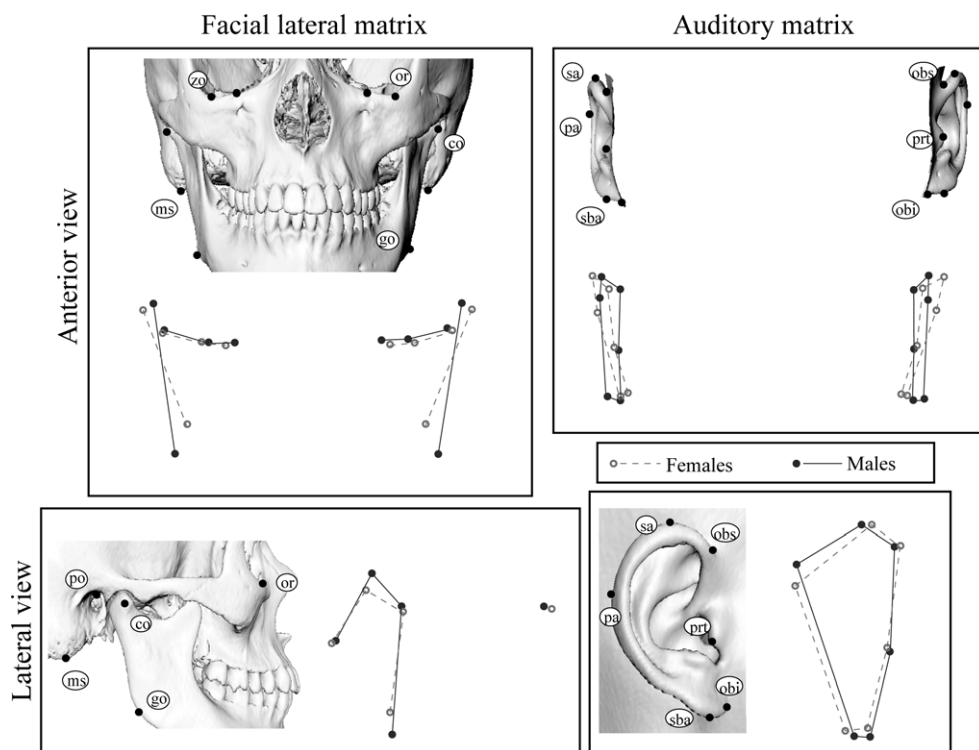
FIG. 7—Sexual dimorphism of the facial lateral and auditory matrices detected by discriminant function analyses. Mean shapes of males and females are superimposed to observe differences.
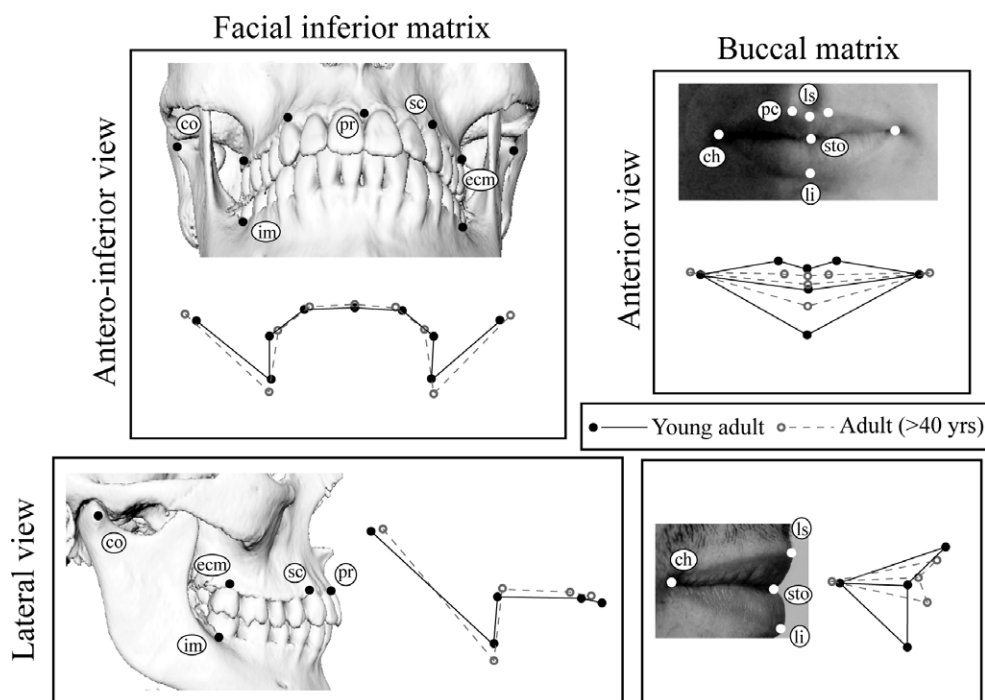

FIG. 8—Age influence of the facial inferior and buccal matrices detected by discriminant function analyses. Mean shapes of individuals younger than 40 years old and individuals older than 40 years old are superimposed to observe differences.

configuration of the target skull, so that the estimated sensory landmarks were directly located in the correct region (eyes, nose, mouth, and ears were treated independently).

The 41 estimated sensory landmarks, along with the 59 FSTD landmarks, created a cloud of 100 points, forming the shape

approximation of the target skull. The transformation of 100 landmarks into a surface was performed using a single generic mesh (Fig. 10), extracted from the MakeHuman© open source tool (version 1.0 *alpha* 6.0; authorization granted by the developers). This face is based upon *c.* 2000 individuals, meaning that
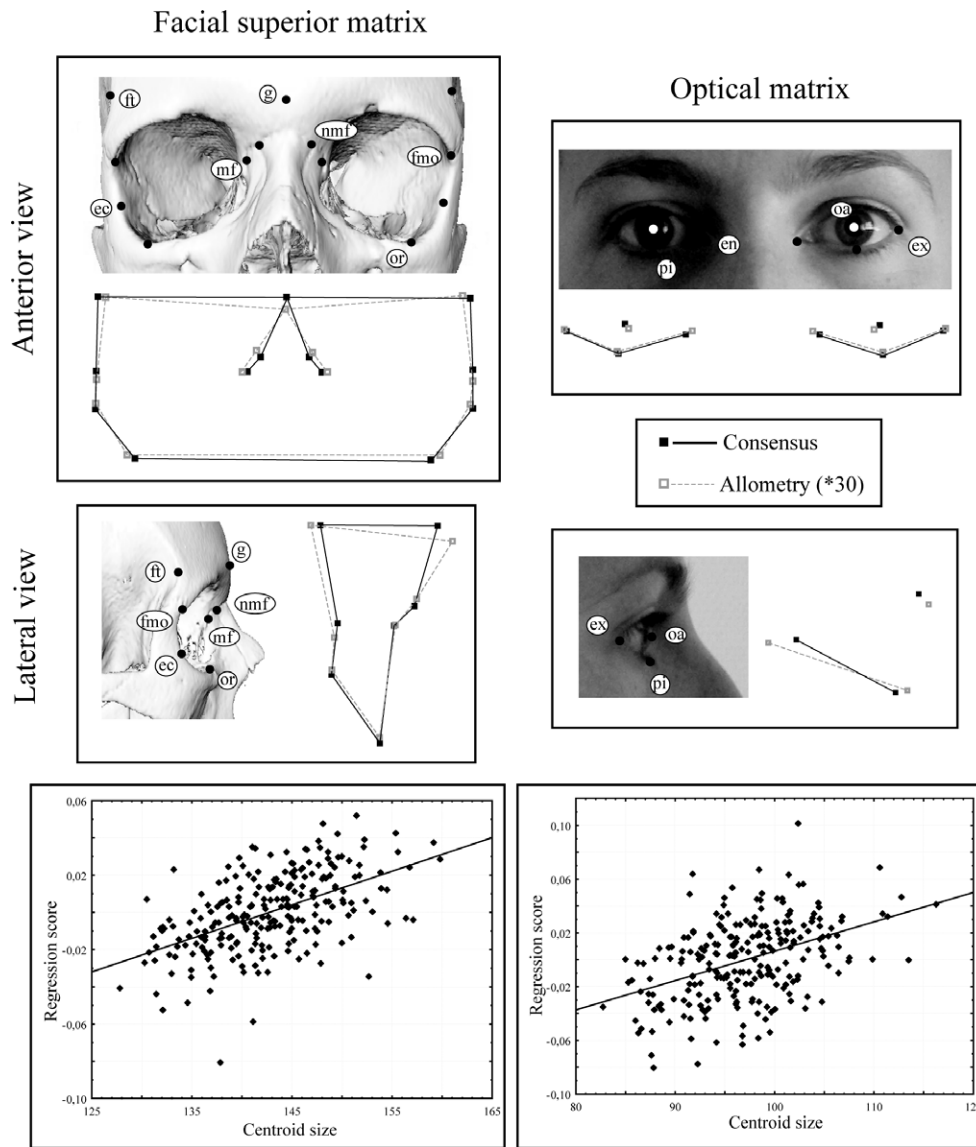
FIG. 9—*Allometric (influence of centroid size on the residuals of the Procrustes superimposition) shape changes on the facial superior and optical matrices. Consensus shapes and accentuated shapes by the allometric factor are superimposed to observe differences.*

TABLE 3—*Statistical results for covariation between bony and cutaneous matrices (PLS), sexual dimorphism (DFA males versus females), age influence (DFA age < 40 years versus age >40 years), and allometry (multivariate regression of size on shape) in the matrices. Bold type: $p < 0.05$.*

MATRIX	Covariation		Sexual dimorphism		Age		Allometry	
	RV	*p*	Mahalanobis	*p*	Mahalanobis	*p*	%	*p*
Facial superior	0.10	**<0.001**	2.509	**<0.001**	1.132	0.425	2.9	**<0.001**
Optical			1.004	**0.012**	1.287	**<0.001**	4.9	**<0.001**
Mid-facial	0.21	**<0.001**	1.298	**0.001**	1.186	**<0.001**	1.4	**0.003**
Respiratory			1.742	**<0.001**	1.837	**0.001**	2.4	**<0.001**
Facial inferior	0.25	**<0.001**	0.936	0.150	1.587	**<0.001**	0.77	0.150
Buccal			0.738	**0.028**	2.041	**0.001**	7.14	**<0.001**
Facial lateral	0.20	**0.002**	2.744	**<0.001**	2.160	**0.003**	3.41	**0.014**
Auditory			2.320	**0.002**	2.338	**<0.001**	8.92	**<0.001**

it provides an objective medium for facial representation, unbiased by specific individual features (e.g., sex, aging marks, hair, etc.). Sensory and FSTD landmarks were positioned on the generic mesh (see Fig. 10) to serve as a guide for the distortion

(i.e., "source" landmarks) of the synthetic face. The sensory landmarks are homologous between individuals, as they are defined on specific anatomical structures. FSTD landmarks are not homologous, as they depend on the position of the bony
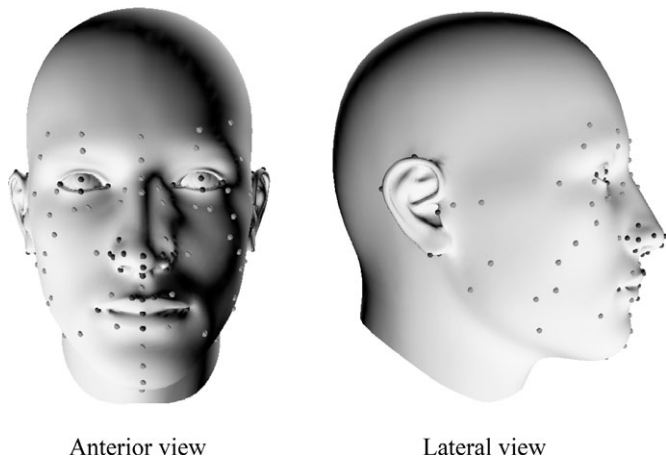
FIG. 10—*Generic base face mesh extracted from the MakeHuman© open source tool, with the source landmarks (light gray = facial soft tissue depth landmarks; dark gray = sensory landmarks).*

underlying landmark, and consequently do not correspond strictly to the same cutaneous locus throughout individuals. For this reason, the distortion was performed in two main phases: a global warping and a local warping. The warping algorithm, developed by one of the authors (JC), was designed as follows:

- Successive translations and rotations are applied to the source landmarks and the corresponding generic face until they best fit with the estimated target landmarks. This step allows for the alignment of the synthetic face on the target skull.
- The iterative algorithm then minimizes the distance between each landmark (source to target). The translations are recorded as vectors and weighted by neighboring landmarks to allow a homogeneous warping. The weighted vectors are applied to the mesh to be warped. This first global warping concerns all 100 landmarks and stops at a specified threshold (e.g., the face will be more accurate with a 0.001 mm limit than a 0.01 mm limit, but will take more time to be warped, and may show small irregularities, known as the Pinocchio effect [16,36]).
- Once the global approximation is obtained, a second operation of warping is performed exclusively on the 41 sensory landmarks. As facial features are more individualizing than FSTD, a higher precision should be achieved regarding their shape. The user can thus set a higher accuracy for this local warping.

The warping operation in AFA3D is able to produce a high variability of facial shapes using a single facial template. Figure 11 presents the anterior view of the 17 test subjects. Eye position, mouth width, nose orientation and width, and overall face shape (round, square, rectangular, etc.) were successfully obtained without un-realistic features due to distortion, as the double warping process allows for the smooth distortion of the outlines. Appearance of the face was somehow similar throughout several individuals as the approximations only provide shape information in 3D; individualization by artistic procedure may be necessary to improve discrimination in perception. The resulting facial approximation can be exported as an individual file to obtain an exploitable face independently from AFA3D by applying skin, eyes, lips color and texture, adding hair and facial hair, aging features, specific jewelry, tattoo, birth mark, or scars depending on the available information for the forensic case, etc.

Test of the Accuracy—The complete set of landmarks for the estimation of the sensory landmarks was collected on 92 individuals of the 500. Using those subjects for which we gathered all the "true" landmarks and the estimated landmarks, it was possible to calculate a mean distance between the true and estimated landmarks after leave-one-out re-sampling (each individual is approximated after being excluded from the reference sample) to obtain an average value for the uncertainty in approximation. The average distances between measured and estimated landmarks based on 92 subjects of the sample are presented in the Table 4. The uncertainty of reconstruction was high for the ear region (7 mm), moderate for the mouth (4.5 mm), and lower for the nasal (3.1 mm) and eye (2.9 mm) regions.

In addition to the mathematical evaluation of AFA3D accuracy, a visual assessment of accuracy was performed by comparing the facial approximation (with the correct age, sex and corpulence) and a warping of the generic face based on the measured landmarks (resulting in the shape the approximation *should* tend to). The two faces, approximated and *true*, were superimposed in AMIRA (version 5.0.1; Mercury Computer Systems, Berlin, Germany) to create a mapping of the differences. This mathematical validation was performed on 17 subjects after leave-one-out re-sampling. Figure 12 displays five examples from the 17 test subjects, with the approximated face, the generic face warped using the measured landmark, and the corresponding map of differences. AFA3D succeeded in approximating the overall shape of the face and the global position and shape of facial organs (e.g., subjects A–D, Fig. 12). Outlier cases with extreme morphology will still be problematic, for example, the subject "e" (Fig. 12) presents evident issues in estimation for FSTD, mouth, ears, and eyes. As all surfaces were warped from the same generic face, the number of vertices is the same throughout the individuals: an average map, based on the errors in approximation for all the 17 test subjects, is presented in Fig. 13. Significant errors of approximation are located on the external ears, the chin, and the temporal region. Due to a lack of landmarks on the cranial vault, the alignment of the model was relatively random on the posterior aspect, which explains high rate of error on the vault and the neck regions.

Discussion

The method behind AFA3D is the first holistic approach using geometric morphometrics and statistical models based on a wide sample (*n* = 500) for facial approximation. The resulting approximations are promising, with an average error of *c.* 4 mm (including FSTD and facial organs). Even if the statistical model can be improved, facial approximation is eventually limited by human variation (e.g., scattering of individuals around regression lines in Figs 7 and 10). Sex, age, corpulence, and centroid size are not the only parameters influencing the facial appearance; other factors need to be assessed to fully understand the individualization of the human face, factors that cannot be easily controlled for or estimated from skeletal remains (i.e., secular trends, diet, environment, biomechanics, muscular activity of the face, etc.) (37–40). Nevertheless, our results indicated significant correlations between bone and soft tissues in terms of shape, which confirmed the first quantified observations made by Simpson and Henneberg (41). It is indeed possible to infer facial appearance using cranial morphology to a certain extent. These authors also stated that differential facial development may induce individualization in specific facial regions (41), underlining the advantage of independent
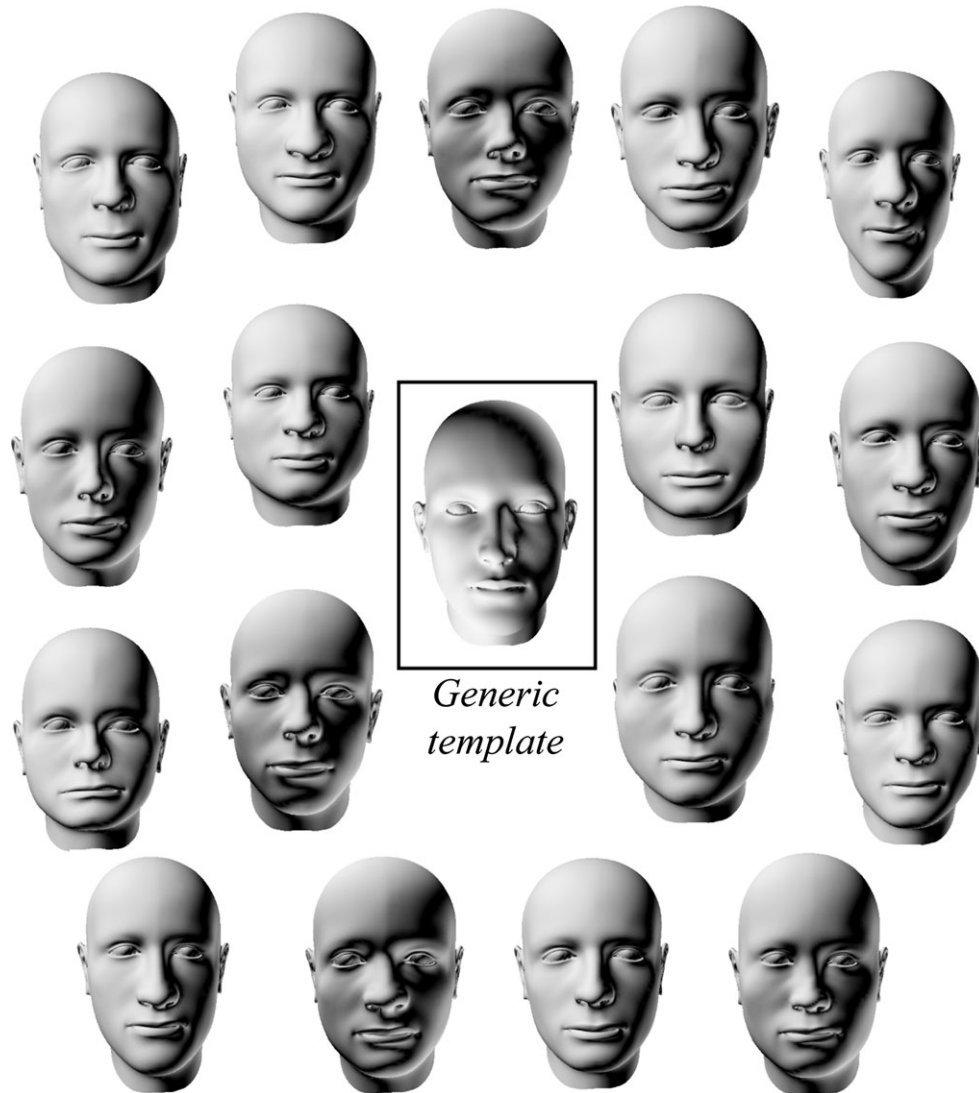
FIG. 11—*The generic facial template (in the center) and the seventeen warped test subjects, showing the shape variations obtained by AFA3D.*

estimations for the different sensory organs of the face in AFA3D.

The accuracy of AFA3D may be improved, especially in the region of the eyes (on which only four landmarks were positioned on each side due to a lack of standardized gaze). The use of outlines and different templates may help improve the accuracy of the estimation for more realistic and specific gazes. The FSTD data applied is specific to the French sample, but because the regressions are built on wide subsamples ($124 < n < 469$), this method might be optimal. Lack of accuracy in the temporal region may be of concern (42), and the chin FSTD estimation should also be improved. However, the application of a single dataset, as in the T-Table (6), may provide similar results in terms of recognition. Even if the population specificity may be less problematic than emphasized by the classic literature regarding FSTD data (22), the question concerning the facial feature shape estimation remains open. Adding individuals of Asian and African ancestry would allow the method to cover a wider range of human facial shape variability. However, the sample used here is representative of the French population and is consequently not limited to Caucasoid individuals. We formulate the following hypothesis (that remains to be tested): as population specificities are characterized in bone facial shape, and AFA3D infers the soft tissue shape using craniometric data, the method should be able to approximate facial features not physically present in the reference sample (i.e., an individual with a nasal aperture larger than any individual of the reference sample of AFA3D will be approximated with a large soft nose width). Performing the facial approximation of a subject of known ancestry with AFA3D can thus be performed using the described process and sample group, with the addition of a specific skin color. Even if the facial soft structure should reflect the facial hard structure through the estimation models for individuals not of French ancestry, adding other population groups in the reference database will, however, eventually improve the results. Different generic facial templates may also be used for flexibility in utilization. Sex- and age-specific faces that include fine textures (i.e., wrinkles) will indeed render more realistic results. Generic faces as the one used by AFA3D may be too smooth and nonspecific for facial recognition (16), but they also might allow for more objectivity in the forensic process.

Overall, the level of precision needed for a facial approximation to result in recognition is not clearly known. The prevalent theory is holistic, implying that the human brain processes at the same time, and with different operations, the shape and position of the organs, the global shape of the face, and facial attributes

TABLE 4—*Uncertainty of approximation (in mm) for each sensory landmark, calculated on 92 individuals after leave-on-out re-sampling.*

Matrix	Landmark	Uncertainty
Optical	Endocanthion	2.6
	Exocanthion	3.2
	Oculus anterior	2.8
	Palpebrale inferior	3.1
	Mean	2.9
Respiratory	Pronasale	3.3
	Inferonasale	3.2
	Midseption	3.0
	Subnasale	2.7
	Alare	3.2
	External alar curv.	3.5
	Superior alar curv.	2.9
	Alagenion	3.1
	Alacrepidon	3.1
	Mean	3.1
Buccal	Labrale superior	4.4
	Labrale inferior	4.6
	Stomion	4.1
	Chelion	4.8
	Philtrum colonna	4.4
	Mean	4.5
Auditory	Otobasion superior	6.2
	Superaurale	7.0
	Postaurale	8.0
	Subaurale	8.3
	Otobasion inferior	7.8
	Protragion	4.7
	Mean	7.0

(texture, color, distinguishing features, etc.) (43,44). The latter elements are defined as high-frequency data, in opposition to the shape and position elements being low-frequency data. It has been hypothesized that relatives (family and close acquaintances) can be recognized through only low-frequency data (e.g., change of hair style/color, makeup, and accessories does not prevent a mother to recognize her daughter) (45–47). In this regard, the information estimated by AFA3D may be useful in forensic cases. Nevertheless, the human brain needs a minimum of basic high-frequency elements to ease the recognition process, and those elements can be added to an AFA3D approximation, as long as they do not bias or mask the estimated shapes (slight skin texture, suggestion of facial hair, etc.) (16,48). An over-abundance of details will indeed hinder recognition, especially if they are not assessed with certainty for a specific case (an example of important high frequencies can be seen in a Roman archaeological facial approximation by Abate et al. [49]). Such assumptions will have to be tested prior to the use of AFA3D in a forensic context.

Conclusion

AFA3D is a computerized facial approximation method allowing for statistical shape estimation of facial morphology using geometric morphometrics based on a French sample of 500 CT-scanned individuals. It uses a holistic approach by combining FSTD and facial organ estimation to produce a cloud of 100 cutaneous landmarks that are transformed into a face through the warping of a single generic template. The accuracy of AFA3D is promising, but needs to be validated with independent samples. AFA3D also fulfills the first objective of facial approximation as defined by the SWGANTH: estimation of antemortem appearance. The second aim, suggesting the identity, involves artistic interpretation of texturing and individualization of the estimation,
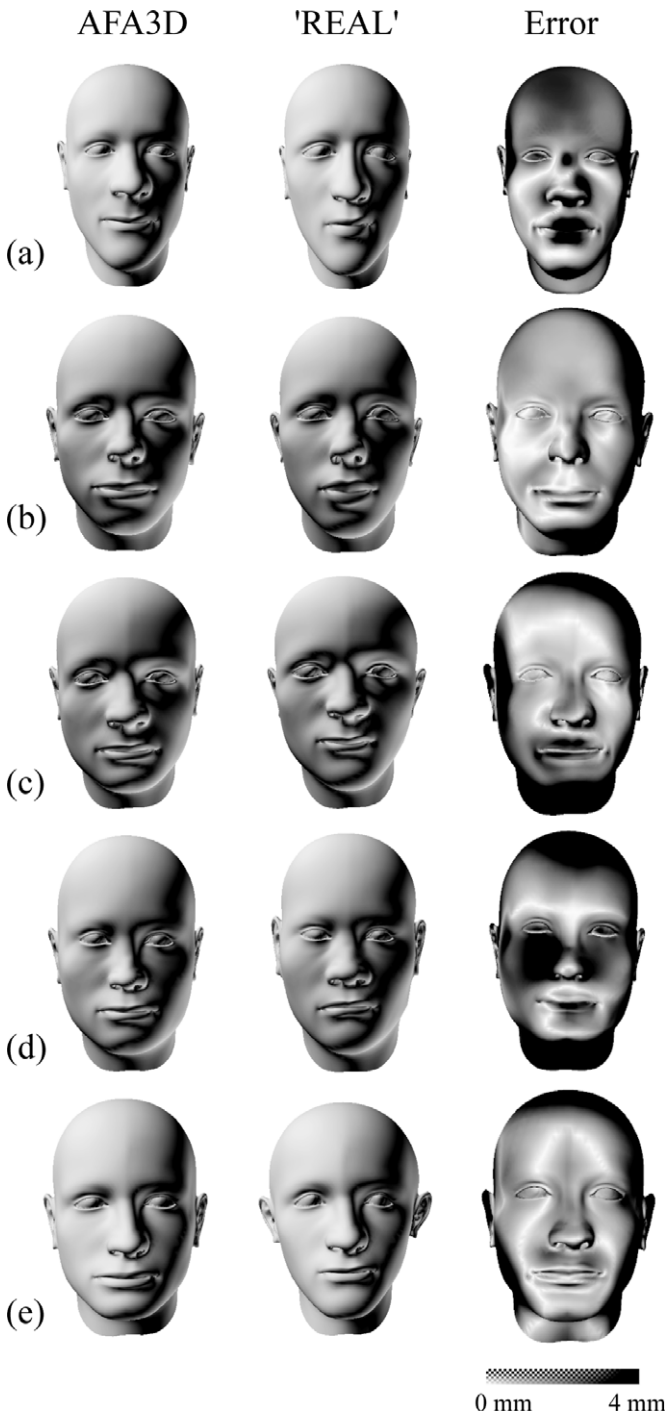

FIG. 12—*Five examples (subjects a to e) of facial approximations performed by AFA3D, confronted with a warping of the generic face using the measured cutaneous landmarks ("real"). The error between the two faces are mapped from no error (in white) to 4 mm of error and more (in black).*

which is necessary for the third goal of capturing public attention regarding the case. Although the model might be improvable, the rendering of the most probable facial shape, as it is in the current version, may already be helpful for recognition. The free online availability of AFA3D will hopefully accelerate testing, validation, and further development through collaborations. The integration of other groups into the reference sample, along with new estimators in the model (in addition to craniometrics, sex, age, and corpulence), is likely to make facial approximation
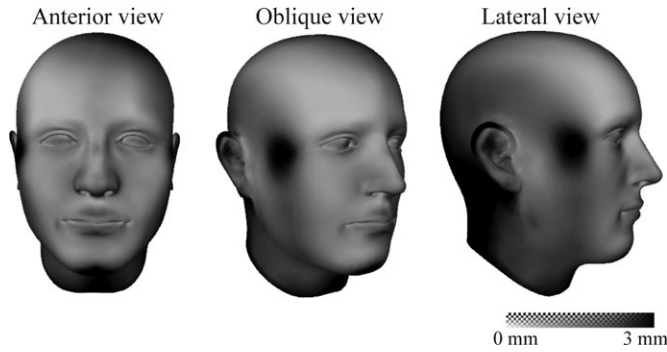
Anterior view Oblique view Lateral view

0 mm   3 mm

FIG. 13—*Average error in the 17 test subjects. White and light gray represent a low error region, versus dark gray and black representing errors of 3 mm and more.*

a powerful tool for identification in forensics. Facial morphology recently began to be explored in terms of genetics (50); future research should focus on gathering information on facial morphology based on the skull architecture and genetic material to propose more accurate and specific facial approximations.

References

1. Tyrrell AJ, Evison MP, Chamberlain AT, Green MA. Forensic three-dimensional facial reconstruction: historical review and contemporary developments. J Forensic Sci 1997;42(4):653–61.
2. Stephan CN. Anthropological facial reconstruction – recognizing the fallacies, 'unembracing' the errors, and realizing methods limits. Sci Justice 2003;43(4):193–200.
3. Verzé L. History of facial reconstruction. Acta Biomed 2009;80(1):5–12.
4. Ullrich H, Stephan CN. On Gerasimov's plastic facial reconstruction technique: new insights to facilitate repeatability. J Forensic Sci 2011;56(2):470–4.
5. De Greef S, Willems G. Three-dimensional cranio-facial reconstruction in forensic identification: latest progress and new tendencies in the 21st century. J Forensic Sci 2005;50(1):12–7.
6. Stephan CN, Simpson EK. Facial soft tissue depths in craniofacial identification (part I): an analytical review of the published adult data. J Forensic Sci 2008;53(6):1257–72.
7. Bruce V, Young A. In the eye of the beholder, the science of face perception. Oxford, UK: Oxford University Press, 1998.
8. Stephan CN, Davidson PL. The placement of the human eyeball and canthi in craniofacial identification. J Forensic Sci 2008;53(3):612–9.
9. Stephan CN, Huang AJR, Davidson PL. Further evidence on the anatomical placement of the human eyeball for facial approximation and craniofacial superimposition. J Forensic Sci 2009;54(2):267–9.
10. Guyomarc'h P, Coqueugniot H, Dutailly B, Couture C. Anatomical placement of the human eyeball in the orbit – new metric data and guidelines proposal for facial identification. Am J Phys Anthropol 2010;141(S50):120.
11. Guyomarc'h P, Stephan CN. The validity of ear prediction guidelines used in facial approximation. J Forensic Sci 2012;57(6):1427–41.
12. Tu PH, Book R, Liu X, Krahnstoever N, Adrian C, Williams P, editors. Automatic face recognition from skeletal remains. Proceedings of the IEEE Conference on Computer Vision and Pattern Recognition; 2007 June 17–22; Minneapolis, MN. Piscataway, NJ: IEEE Press, 2007;1–7.
13. Tu PH, Hartley R, Lorensen W, Allyassin M, Gupta R, Heier L. Face reconstruction using flesh deformation modes. In: Clement JG, Marks MK, editors. Computer-graphic facial reconstruction. Burlington, MA: Elsevier Academic Press, 2005;145–62.
14. Kustar A, Forro L, Kalina I, Fazekas F, Honti S, Makra S, et al. FACE-R – a 3D database of 400 living individuals' full head CT- and face scans and preliminary GMM analysis for craniofacial reconstruction. J Forensic Sci 2013;58(6):1420–8.
15. Parks CL, Richard AH, Monson KL. Preliminary performance assessment of computer automated facial approximations using computed tomography scans of living individuals. Forensic Sci Int 2013;233(1–3):133–9.
16. Claes P, Vandermeulen D, De Greef S, Willems G, Clement JG, Suetens P. Computerized craniofacial reconstruction: conceptual framework and review. Forensic Sci Int 2010;201(1–3):138–45.
17. Guyomarc'h P. Reconstitution faciale par imagerie 3D: variabilité morphométrique et mise en oeuvre informatique. Talence, France: Université de Bordeaux, 2011.
18. Spoor CF, Zonneveld FW, Macho GA. Linear measurements of cortical bone and dental enamel by computed tomography: applications and problems. Am J Phys Anthropol 1993;91(4):469–84.
19. Dutailly B, Coqueugniot H, Desbarats P, Gueorguieva S, Synave R. 3D surface reconstruction using HMH algorithm. Proceedings of the 16th IEEE International Conference on Image Processing (ICIP09); 2009 Nov 7-11; Cairo, Egypt. Piscataway, NJ: IEEE Press, 2009;2505–8.
20. Guyomarc'h P, Santos F, Dutailly B, Desbarats P, Bou C, Coqueugniot H. Three-dimensional computer-assisted craniometrics: a comparison of the uncertainty in measurement induced by surface reconstruction performed by two computer programs. Forensic Sci Int 2012;219(1–3):221–7.
21. Bookstein FL. Introduction to methods for landmark data. In: Rohlf FJ, Bookstein FL, editors. Proceedings of the michigan morphometrics workshop; 1990 May 16–28; Ann Arbor, MI. Ann Arbor, MI: University of Michigan Museum of Zoology, 1990;215–25.
22. Guyomarc'h P, Santos F, Dutailly B, Coqueugniot H. Facial soft tissue depths in French adults: variability, specificity and estimation. Forensic Sci Int 2013;3:411e1–10.
23. Inserm, TNS Healthcare (KANTARHEALTH), Roche. Obépi – Enquête épidémiologique nationale sur le surpoids et l'obésité, 2009, http://www.arp-probs.fr/wp-content/uploads/2012/09/obepi-2009.pdf.
24. Rohlf FJ, Marcus LF. A revolution in morphometrics. Trends Ecol Evol 1993;8(4):129–32.
25. Richtsmeier JT, Deleon VB, Lele SR. The promise of geometric morphometrics. Yearb Phys Anthropol 2002;1(1 suppl):63–91.
26. Adams DC, Rohlf FJ, Slice DE. Geometric morphometrics: ten years of progress following the 'revolution'. Ital J Zool 2004;71(1):5–16.
27. Mitteroecker P, Gunz P. Advances in geometric morphometrics. Evol Biol 2009;36(2):235–47.
28. Klingenberg CP. MorphoJ: an integrated software package for geometric morphometrics. Mol Ecol 2010;11(2):353–7.
29. Moss ML, Young RW. A functional approach to craniology. Am J Phys Anthropol 1960;18(4):281–92.

30. Robert P, Escoufier Y. A unifying tool for linear multivariate statistical methods: the RV coefficient. Appl Stat 1976;25(3):257–65.

31. Rohlf FJ, Corti M. Use of two-block partial least-squares to study covariation in shape. Syst Biol 2000;49(4):740–53.

32. Klingenberg CP, Badyaev AV, Sowry SM, Beckwith NJ. Inferring developmental modularity from morphological integration: analysis of individual variation and asymmetry in Bumblebee wings. Am Nat 2001;157 (1):11–23.

33. Klingenberg CP. Morphometric integration and modularity in configurations of landmarks: tools for evaluating a priori hypotheses. Evol Dev 2009;11(4):405–21.

34. Velemínská J, Bigoni L, Krajíček V, Borský J, Šmahelová D, Cagáňová V, et al. Surface facial modelling and allometry in relation to sexual dimorphism. HOMO 2012;63(2):81–93.

35. R Development Core Team. R: a language and environment for statistical computing. Vienna, Austria: R Foundation for Statistical Computing, 2010.

36. Zelditch ML, Swiderski DL, Sheets HD, Fink WL. Geometric morphometrics for biologists: a primer. Amsterdam, Boston: Elsevier Academic Press, 2004.

37. Jantz RL, Meadows-Jantz L. Secular change in craniofacial morphology. Am J Hum Biol 2000;12:327–38.

38. Evison M, Dryden I, Fieller N, Mallett X, Morecroft L, Schofield D, et al. Key parameters of face shape variation in 3D in a large sample. J Forensic Sci 2009;55(1):159–62.

39. Mallett X, Dryden I, Vorder Bruegge R, Evison M. An exploration of sample representativeness in anthropometric facial comparison. J Forensic Sci 2010;55(4):1025–31.

40. Curtis N. Craniofacial biomechanics: an overview of recent multibody modelling studies. J Anat 2011;218(1):16–25.

41. Simpson E, Henneberg M. Variation in soft-tissue thicknesses on the human face and their relation to craniometric dimensions. Am J Phys Anthropol 2002;118(2):121–33.

42. Stephan CN, Devine M. The superficial temporal fat pad and its ramifications for temporalis muscle construction in facial approximation. Forensic Sci Int 2009;191(1):70–9.

43. Dekowska M, Kuniecki M, Jaskowski P. Facing facts: neuronal mechanisms of face perception. Acta Neurobiol Exp 2008;68(2):229–52.

44. Smeets D, Claes P, Vandermeulen D, Clement JG. Objective 3D face recognition: evolution, approaches and challenges. Forensic Sci Int 2010;201(1–3):125–32.

45. Roessli DC. Approche morphométrique dans l'étude de la perception et de la reconnaissance du visage humain. Genève, Switerland: Université de Genève, 1998.

46. Sinha P, Balas BJ, Ostrovsky Y, Russel R. Face recognition by humans: 19 results all computer vision researchers should know about. Proc IEEE 2006;94(11):1948–62.

47. Lewandowski Z, Pisula-Lewandowska A. The influence of change in the size of face elements on the perception of a woman's portrait. HOMO 2008;59(3):253–60.

48. Wilkinson CM. Facial reconstruction – anatomical art or artistic anatomy? J Anat 2010;216(2):235–50.

49. Abate AF, Nappi M, Ricciardi S, Tortora G. FACES: 3D FAcial reConstruction from anciEnt Skulls using content based image retrieval. J Visual Lang Comput 2004;15(5):373–89.

50. Liu F, van der Lijn F, Schurmann C, Zhu G, Chakravarty MM, Hysi PG, et al. A genome-wide association study identifies five loci influencing facial morphology in Europeans. PLoS Genet 2012;8(9):e1002932.

Additional information and reprint requests:
Pierre Guyomarc'h, Ph.D.
Université Bordeaux 1
UMR 5199 PACEA - A3P
Allée Geoffroy Saint Hilaire, Bat B8
CS 50023 33615 Pessac Cedex
France
E-mail: pierreguyo@gmail.com